

# Free Volume Distributions in Ultrahigh and Lower Free Volume Polymers: Comparison between Molecular Modeling and Positron Lifetime Studies

D. Hofmann,<sup>\*,†</sup> M. Heuchel,<sup>†</sup> Yu. Yampolskii,<sup>‡</sup> V. Khotimskii,<sup>‡</sup> and V. Shantarovich<sup>§</sup>

*Institute of Chemistry, GKSS Research Center, Kantstrasse 55, D-14513 Teltow, Germany;  
A. V. Topchiev Institute of Petrochemical Synthesis, Russian Academy of Sciences, 29 Leninsky Pr.,  
117912 Moscow, Russia; and N. N. Semenov Institute of Chemical Physics, Russian Academy of  
Sciences, 4 Kosygina Str., 117334 Moscow, Russia*

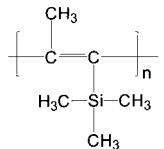
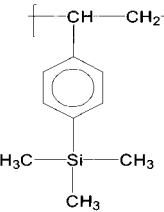
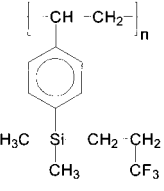
*Received July 30, 2001; Revised Manuscript Received November 28, 2001*

**ABSTRACT:** The present paper deals with important differences in the distribution of free volume in high and low free volume polymers as indicated by a joint investigation utilizing molecular modeling and positron annihilation lifetime studies. The main focus of this paper is on the molecular modeling approach. The polymers in question are the ultrahigh free volume polymer poly(1-(trimethylsilyl)-1-propyne) (PTMSP) and two polystyrene derivatives containing Si and F. Extended equilibration procedures were necessary to obtain reasonable packing models for the polymers. The transition state Gusev–Suter Monte Carlo method was utilized to prove a reasonable agreement between simulated and measured diffusivity and solubility values for the model structures. The free volume distribution was analyzed for the validated packing models and compared with respective positron annihilation data. In both cases, a bimodal distribution of free volume was observed for PTMSP while the polystyrene derivatives as other conventional glassy polymers showed a more or less monomodal behavior. Good qualitative agreement is demonstrated between size distributions of free volume elements in these polymers obtained via molecular computer modeling and experiments using positron annihilation technique.

## 1. Introduction

The free volume distribution in amorphous polymers is of paramount importance for their transport behavior toward small- and medium-sized penetrant molecules. There are several experimental methods to characterize the free volume of a polymer: among them are photochromic<sup>1</sup> and spin<sup>2</sup> probe methods as well as inverse gas chromatography.<sup>3</sup> However, positron annihilation lifetime spectroscopy (PALS) should be considered as the method that gives the most direct and detailed information on free volume.<sup>4</sup> Every probe method has some limitations, which are related to necessary prerequisites for the evaluation of the measured data. For instance, in most PALS studies simple spherical shapes are assumed for the individual holes (microcavities) forming the free volume. As will be subsequently shown, this is not in line with results of molecular modeling simulations. The data obtained by probe methods have been only very rarely compared with the results of computer simulation of polymer nanostructure. In this paper, it is assumed that combined PALS and molecular modeling studies can provide a better insight into the distribution of free volume in amorphous polymers. For this purpose, three polymers are considered: poly(1-(trimethylsilyl)-1-propyne) (PTMSP)<sup>6–17</sup> as a typical high free volume, highly permeable glassy polymer and two Si- and F-containing polystyrene derivatives,<sup>18</sup> which show only moderately high gas permeability. Their chemical structures and some properties are presented in Table 1.

**Table 1. Structure and Properties of the Polymers<sup>a</sup>**

Polymer	Formula	Density, g/cm <sup>3</sup>	FFV, %	T <sub>g</sub> , °C
PTMSP		0.75 (ref. <sup>10,11</sup> )	33	>200°C (ref. <sup>6,11</sup> )
PTMSS		0.965 (ref. <sup>18</sup> )	20	135 (ref. <sup>18</sup> )
PFPDMSS		1.127 (ref. <sup>18</sup> )	18	62 (ref. <sup>18</sup> )

<sup>a</sup> FFV = fractional free volume estimated from Bondi method; T<sub>g</sub> = glass transition temperature.

PTMSP was first described by Masuda et al.<sup>5,6</sup> This polymer is amorphous and has a glass transition temperature above 250 °C. In many aspects, it is distinguished by unusual properties. First, it is the most permeable polymer known.<sup>7,8</sup> For this polymer, higher

\* To whom correspondence should be addressed.

<sup>†</sup> GKSS Research Center.

<sup>‡</sup> A. V. Topchiev Institute of Petrochemical Synthesis, Russian Academy of Sciences.

<sup>§</sup> N. N. Semenov Institute of Chemical Physics, Russian Academy of Sciences.

permeability is observed with respect to larger, more condensable penetrants molecules such as butane than to light gases such as He or H<sub>2</sub>, a behavior typical for rubbery and not glassy polymers.<sup>9</sup> Negative activation energies of permeation through this material are obviously a consequence of unusually low activation energies of diffusion observed for PTMSP.<sup>8</sup> These and some other exceptional permeation properties, which are in sharp contrast to those of conventional amorphous polymers, are usually attributed to the very low density of "freshly cast" PTMSP films. It was determined<sup>10,11</sup> to be between 0.7 and 0.8 g/cm<sup>3</sup> and shows remarkable aging to values of about 0.95 g/cm<sup>3</sup> already a few months after the membrane formation. Simultaneously, gas permeability is rapidly reduced by up to 2 orders of magnitude.<sup>12</sup> This very low density of the as-prepared PTMSP films reveals an extremely high fractional free volume (FFV), which was estimated using group contribution methods as about 0.3. The presence of high free volume and microheterogeneity (i.e., the presence of a partly continuous hole phase) in PTMSP were also confirmed by probe methods.<sup>13,14</sup> As possible causes, mainly the rigid backbone, the very bulky and symmetrical trimethylsilyl side chains, and the presence of a methyl group attached to another C atom of the main chain, which prevents rotation around a single C–C bond, were discussed.<sup>7,10,11,15</sup> Free volume and its size distribution can depend on spatial orientation of the main chains, that is, on the cis/trans ratio and the sequence of corresponding subunits of the main chain.<sup>16,17</sup> In the present work, we deal with PTMSP prepared with TaCl<sub>5</sub> catalyst. The resulting structure consists of random sequence of cis and trans configurations with approximately the same content.<sup>16</sup> The same configuration was employed in a computer simulation of this polymer.

Two polystyrene derivatives studied, poly(*p*-trimethylsilylstyrene) (PTMSS) and poly(*p*- $\gamma$ -trifluoropropyl-dimethylsilylstyrene) (PFPMSS) were prepared by radical polymerization in the presence of 2,2-azobisisobutyronitrile.<sup>18</sup> In contrast to PTMSP, they do not reveal high gas permeability though both contain bulky silyl-substituted side groups. Their permeability is only one order larger than that of polystyrene.

Molecular modeling investigations can tackle the problem of free volume characterization from the theoretical end. These techniques have been widely used over the past decade to get a deeper insight in the structure and the transport behavior of nonporous amorphous polymer membranes. General results of these investigations can be found, e.g., in a number of reference and feature articles.<sup>19–21</sup> Findings of molecular modeling simulations, specifically on the ultrahigh free volume polymer PTMSP and related materials, have recently been published by Fried<sup>22</sup> et al., Madkour,<sup>23</sup> and Hofmann et al.<sup>21</sup> Fried et al. created a large number (100) of rather small packing models each containing only 50 PTMSP repeat units. Densities between 0.80 and 0.85 g/cm<sup>3</sup> were reported for the completely equilibrated packing models. Sorption and diffusion mechanisms for small gas molecules were investigated. In general, a reasonable coincidence with related experimental data was reported.

Madkour<sup>23</sup> on the other hand used molecular modeling techniques to follow the aging process (see above) of as prepared PTMSP films. For this purpose he built and characterized relatively small (50 repeat units) packing models for a series of modified PTMSP struc-

tures, e.g., showing only single bonds in the backbone or a carbon atoms instead of the silicon atoms etc. and followed the development of simulated density and diffusivity values.

Hofmann et al.<sup>21</sup> also investigated the aging behavior of PTMSP. There in difference to the just mentioned papers a small number of relatively large models containing about 9500 atoms were built at a density of 0.75 g/cm<sup>3</sup> (representative for as-cast PTMSP films). The models were then subjected to sequences of stimulated annealing under *NVT* (*NVT* = constant particle number *N*, constant volume *V*, and constant temperature *T*) conditions at 600 K and *NPT* (*NPT* = constant particle number *N*, constant pressure *P*, and constant temperature *T*) runs at 1 bar and 303 K. The result was a clear tendency of a density increase toward about 0.95 g/cm<sup>3</sup>, a value typical for PTMSP membranes of a few months age.

Comparisons between positron annihilation and molecular modeling studies have hitherto only rarely been reported. A paper of Nagel et al.<sup>24</sup> dealt with the investigation of free volume in a number of glassy polyimides and rubbery poly(dimethylsiloxane)s. Asymmetric, decreasing hole size distributions indicating the presence of nonspherical holes were detected. Furthermore, it was concluded that the positrons traveling through the respective polymer matrix detect not only just the distribution of free volume but also the dynamics of the polymer matrix. Here it should be mentioned that as could be shown by molecular-dynamics (MD) simulations,<sup>21,25,26</sup> besides the free volume distribution, the dynamic behavior of membrane polymers as well is of decisive importance for their transport properties toward small- and medium-sized molecules. A similar conclusion was reached in a recent study<sup>27</sup> of various polyacetylenes using the spin probe method.

Schmitz et al.<sup>28</sup> used packing models for amorphous polymers obtained from MD procedures. They then calculated the quantum mechanical density of positronium in a given polymer matrix utilizing a quantum path integral Monte Carlo method where the polymer provided for the background potential. In this way they could get much better coincidence with experimental PAL data, than by making the common approximation of the free volume being organized in spherical holes.

## 2. Modeling Details

For each of the polymers PTMSP, PTMSS, and PFPMSS three independent atomistic bulk models were realized utilizing the Amorphous Cell module of the InsightII/Discover Software of Molecular Simulations Inc.<sup>29</sup> The basic techniques used are described in ref 21.

For PTMSP, the initial packing procedure was performed with an atactic chain of 499 repeat units (9483 atoms) with a 50:50 probability for the occurrence of monomers with cis and trans configurations at a density of 0.75 g/cm<sup>3</sup>. It can be assumed that for stiff chain polymers (and PTMSP is an example of a polymer with extremely stiff chains) the effects of spatial nonuniformity would escape when modeling with relatively short chains. Because of it, in the present work, we consider the PTMSP chains longer by almost an order of magnitude than those which have been dealt with in some of the earlier works<sup>22,23</sup> on simulation of this polymer. However, it must be stressed that considering the high degree of stiffness of PTMSP chains our models are still

**Table 2. Scaling of Conformation Energy Terms and Nonbonded Interaction Energy Terms in the Forcefield for the Equilibration of the PTMSP Models<sup>a</sup>**

stage of equilibration	scaling factor for the conformation energy terms in the force field	type of nonbonded interaction energy terms	scaling factor for the nonbonded interaction energy terms
1	0.001	6–9 potential + Coulomb	0.001
2	0.1	6–9 potential + Coulomb	0.001
3	1	6–9 potential + Coulomb	0.001
4	1	6–9 potential + Coulomb	0.01
5	1	6–9 potential + Coulomb	1

<sup>a</sup> All stages were performed under *NVT* (constant particle number *N*, constant volume *V*, and constant temperature *T*) conditions.

relatively small, a problem that in the present study could not be overcome with the available state of the art soft- and hardware. Considering the positive results of comparisons with experimental data (reported below), we are however confident that the simulated PTMSP models are of reasonable relevance for the characterization of basic features of the free volume distribution.

A selection having a cis/trans ratio of 50/50 makes it possible to compare the predicted parameters with the experimental ones. The side length of the resulting packing cell was 49.9 Å. As force field the newly developed COMPASS force field of Molecular Simulations was used.<sup>30,31</sup> The resulting initial packing models were equilibrated according to the procedure outlined in Table 2.

The individual stages lasted for 5000–10000 ps and were always preceded by a short energy minimization of several hundred iterations. Afterward, a 50 ps MD run was performed for each of the models in order to further improve the equilibration. Three independent packing models, PTMSP-1, PTMSP-2, and PTMSP-3, were constructed for PTMSP. These models correspond to three different possible local chain segment assemblies of PTMSP.

Since PTMSS and PFPDMSS contain cyclic subunits (here, phenylene rings) in the repeat units, the packing and equilibration stages have been much more laborious and time-consuming than in the case of PTMSP (cf., e.g., refs 21 and 26). For such systems, the packing algorithm may lead to artifacts of catenated phenylene rings or a spearing of side groups or backbone chains through ring sub-structures. Both effects are, of course unacceptable and have to be avoided. To solve this technical problem, it is usually necessary to start with a very low initial packing density (typically 0.1 g/cm<sup>3</sup>). For PTMSS and PFPDMSS, this approach alone did not, however, lead to a complete avoiding of catenation and spearing events. Therefore, an alternative technique was chosen, where in all the cases the already mentioned Compass force field was used.

Again, three independent packing models were constructed in each case. There for the initial packing algorithm the experimental densities (0.965 and 1.127 g/cm<sup>3</sup> for PTMSS and PFPDMSS, respectively) were

applied. The basic volume element of packing was filled with 8402 atoms (300 repeat units in the atactic sequence) for PTMSS and 8502 atoms (250 repeat units in the atactic sequence) for PFPDMSS. Before, in each case, 100 methanol molecules were inserted in the respective packing cell. This procedure aims at forming small obstacles, preventing the respective growing polymer chains from ring catenations and spearings. The obstacle molecules are later of course to be removed again. This technique was first utilized for the simulation of polyimides.<sup>32</sup>

All initial packing models obtained in this way were subsequently subjected to the same equilibration procedure as the PTMSP packing models (cf. Table 2). Afterward the first 50 and later the second 50 methanol molecules were removed from each packing model followed at each case by an additional equilibration. To avoid the creation of new catenation problems, these equilibrations were performed with a stimulated annealing procedure (cf. Table 3) instead of the force field parameter scaling described before. As in the case of PTMSP, each individual stage lasted for 5000–10000 ps and the 303 K stage was always preceded by a short energy minimization of several hundred iterations.

Due to the removal of the methanol molecules, the resulting systems were slightly below the respective experimental densities (0.91 g/cm<sup>3</sup> for PTMSS and 1.074 g/cm<sup>3</sup> for PFPDMSS). Therefore, at this stage the systems were simulated for 5000 ps under high pressure at 1000–5000 bar via *NPT*–MD dynamics followed by a stimulated annealing procedure similar to the one shown in Table 3. By modifying the pressure and temperature parameters it was attempted to bring the packing models closer to the experimental densities under conditions of a 1 bar with *NPT*–MD simulation. For PTMSS only 95% of the experimental density was achieved at 1 bar. Slight problems such as this may happen for glassy stiff chain materials (cf. refs 26, 29, and 33), particularly if the models are rather large, as in the given case. These deviations may reflect minor errors of the parametrization of the respective polymers in the chosen force field which influence the equilibration of the respective model. The whole procedure gets tougher, the stiffer the chain and the larger the model. In these cases of relatively low deviations of the model density at a 1 bar *NPT*–MD simulation from the respective experimental value, it is usually no problem to recompress the model to the experimental density and to run all subsequent MD simulations in the *NVT* mode. The resulting side length of the PTMSS packing models was 45.0 Å.

For PFPDMSS, it was possible to reach a 1 bar simulated density of 96–98% of the experimental value. Therefore, in this case only the packing models PFPDMSS-1 and PFPDMSS-2 were afterward simulated at the exact experimental value under *NVT* conditions while for the sake of comparison the model PFPDMSS-3 was subsequently always treated under *NPT*. The side length of the resulting packing cells was 45.7 Å for PFPDMSS-1 and PFPDMSS-2 and 45.9 Å for PFP-

**Table 3. Stimulated Annealing Equilibration Procedure**

stage of equilibration	status of <i>p</i> and <i>T</i>	scaling factor for conformation energy terms in the force field	type of nonbonded interaction energy terms in the force field	scaling factor for atomic radii in nonbonded interaction energy terms	time step in fs
1	<i>NVT</i> , 600 K	1	6–9 potential + Coulomb	1	0.5
2	<i>NVT</i> , 303 K	1	6–9 potential + Coulomb	1	1

DMSS-3. Before any further evaluation of the models, each model was subjected to an additional 200–300 ps of MD simulation.

### 3. Experimental Section

PTMSP has been studied extensively, so its transport parameters reported by several authors were taken from the literature. The synthesis of the investigated polymers PTMSS and PFPDMSS as well as the determination of macroscopic transport properties have been described in detail before<sup>18</sup> and will not be recalled here. Some of the properties of the polymers studied are given in Table 1. Here the fractional free volume  $FFV = V_f/V_{sp}$  was estimated using experimental density  $\rho$  and van der Waals volumes  $V_w$  of the atoms forming the repeat units. According to the Bondi method<sup>34</sup> free volume of a polymer  $V_f$  (cm<sup>3</sup>/g) can be estimated as

$$V_f = V_{sp} - 1.3 V_w \quad (1)$$

where the specific volume  $V_{sp}$  is defined as reciprocal density ( $1/\rho$ ), the van der Waals volume can be calculated using a group contribution method, and a universal “packing coefficient” equal to 1.3 is used to convert the van der Waals volume of the repeat unit in the occupied volume. The correctness of this approach for all the polymers and in relation to transport of various gases has been discussed (see, e.g., ref 35). It can be assumed that a large scatter of the empirical correlations of diffusion and permeability coefficients with  $V_f$  and FFV often observed for various polymers can be induced by the only approximate validity of these equations.

Free volume and its size distribution in the polymers under investigation was also determined using positron annihilation lifetime spectroscopy. The PAL spectra were measured at room temperature with a conventional Ortec “fast-fast” lifetime spectrometer. The time resolution was 230 ps (fwhm). A nickel-foil-supported [<sup>22</sup>Na]-sodium chloride radioactive source of positrons was used. The contribution from the annihilation in the source material, a background, and instrumental resolution were taken into account. Inverse Laplace transformation of the PAL spectra using the CONTIN program<sup>36,37</sup> was employed for obtaining a continuous lifetime and free volume size distributions. It should be emphasized that this program selects automatically the number of components in the PAL spectrum. Each final PAL spectrum was obtained by summing up the results of several cycles of measurements (10<sup>6</sup> counts in each cycle). The integral statistics for each spectrum was equal to  $(1.5-2.0) \times 10^7$  coincidences, and this spectrum was used for CONTIN analysis. CONTIN program determined the “chosen solution”, corresponding to regularization parameter  $\alpha \sim 10^{-4}$ . This is a solution having a Fisher  $F$ -probability closest to 0.5.

It has been shown<sup>14</sup> that measurements of positron annihilation lifetimes, when the sample is under ambient conditions, can lead to erroneous results in determination of free volume due to an additional channel of o-positronium annihilation caused by interaction with sorbed oxygen. This effect is especially dramatic for high volume polymers. To avoid these complications the investigation of free volume was carried out in the absence of oxygen. For this purpose, the measurements were performed in an inert (nitrogen) atmosphere, the samples being kept in a stream of dry nitrogen in a polyethylene hose.

### 4. Results and Discussion

**4.1. Validation of the Packing Models.** To validate the quality of the obtained equilibrated packing models against experimental data the Gusev–Suter method<sup>38,39</sup> was applied to obtain simulated constants of diffusion and solubilities for the gases O<sub>2</sub>, N<sub>2</sub>, CH<sub>4</sub> and CO<sub>2</sub>. Tables 4 and 5 contain a comparison between these parameters and respective experimental results for “as-prepared” (nonaged) PTMSP films as well as PTMSS and PFPDMSS films. For the gas pair O<sub>2</sub>/N<sub>2</sub> a compari-

son is also shown for the selectivity of sorption and diffusion found experimentally and calculated.

Before discussing these Tables, it is necessary to outline briefly the basics of the Gusev–Suter method. There the interaction energy of an inserted test gas molecule of a given kind is calculated on each position of a fine grid layered over an amorphous packing cell. For this purpose just the Lennard-Jones and not the Coulomb interaction energy is considered. Furthermore it is assumed that the polymer packing does not have to undergo structural relaxation (e.g., resulting from torsion transitions) to accommodate an inserted particle. Therefore, this simulation technique is restricted to small molecules (up to methane or even just N<sub>2</sub>) which do not show significant electrostatic interactions with a polymer matrix. Using these energy values, first the solubility of the respective gas can be estimated (cf. refs 21, 38, 39). In addition, the whole packing can be separated in regions of free volume (sites of low interaction energy) and regions of densely packed polymer (high interaction energy). After this, energetically favorable transition paths between adjacent sites are identified. Each path gets a Boltzmann factor of jump probability assigned, which results from proper averaging over the insertion energies determined in the area between the two sites connected by that path. The jump probabilities are also influenced by the elastic thermal vibrations of the polymer matrix. This effect is considered via a Debye-like factor. The main material parameter utilized in this context is  $\langle \Delta^2 \rangle$ , the mean squared displacement (fluctuation) of a polymer atom from its average position. Usually, this quantity amounts to a fraction of an angstrom. For the sake of the study reported here, the smearing factor  $\langle \Delta^2 \rangle$ , was determined via the so-called self-consistent field procedure<sup>39</sup> employing the mean squared displacement  $s(t)$  of the respective polymer atoms. The function  $s(t)$  was obtained from 20 ps MD runs for the respective polymer packing model with snapshots taken every 100 fs.

Having determined appropriate jump probabilities, the diffusion of gas particles can then be simulated via an MC type procedure. The main advantage of this method is that much less computer time is consumed then for a full detailed-atomistic MD simulation, which requires much longer simulation times.

When considering the results shown in Tables 4 and 5, it should be noted that the possible deviations of predicted solubility and diffusivity data can be relatively high for glassy stiff chain polymers as compared with the experimental values. This is partly also due to the difficulties in experimentally obtaining really amorphous polymeric materials and accurate measurements of  $D$  and  $S$  values. In other words, all the glassy polymers are inherently nonequilibrium structures. Thus each individual film produced may have an individual deviation from the respective ideal equilibrated state. In addition, the relations between the gas molecule insertion energies determined directly from the packing models and the quantities  $D_{\text{calcd}}$  and  $S_{\text{calcd}}$  are highly complex. Therefore, even relatively small errors of the insertion energies which are determined by the quality of a respective model may lead to rather high errors for  $D_{\text{calcd}}$  and  $S_{\text{calcd}}$ . Because of both reasons, it is generally accepted that a coincidence between measured and simulated diffusivity and solubility values within a factor of 3–5 is still reasonable (cf., e.g., ref 19). For the given rather large packing models a further techni-

**Table 4. Comparison of Calculated and Experimental Transport Properties for PTMSP**

solubility coefficient, $S$ [cm <sup>3</sup> (STP)/(cm <sup>3</sup> atm)]				selectivity:solubility ratio O <sub>2</sub> /N <sub>2</sub>	model (ref)
O <sub>2</sub>	N <sub>2</sub>	CO <sub>2</sub>	CH <sub>4</sub>		
1.36	1.14	10.2	2.8	1.19	PTMSP-1
1.39	1.16	8.5	2.8	1.20	PTMSP-2
1.43	1.19	8.8	2.9	1.20	PTMSP-3
1.26	1.08	8.05	3.74	1.17	(10) <sup>a</sup>
1.06	1.08	10.2	3.80	0.98	(40)
n.a.	0.91	5.8	2.05	n.a.	(8) <sup>b</sup>

diffusion coefficient, $D$ [10 <sup>-5</sup> cm <sup>2</sup> /s]				selectivity:diffusion ratio O <sub>2</sub> /N <sub>2</sub>	model (ref)
O <sub>2</sub>	N <sub>2</sub>	CO <sub>2</sub>	CH <sub>4</sub>		
3.6	1.5	0.8	1.7	2.40	PTMSP-1
10.6	13.1	4.7	12.4	0.81	PTMSP-2
8.2	8.3	4.4	10.5	0.99	PTMSP-3
4.65	3.5	2.64	2.64	1.33	(10) <sup>c</sup>
3.58	2.55	2.17	2.27	1.40	(10) <sup>d</sup>
2.2	1.5	2.5	1.63	1.47	(8)

<sup>a</sup> Direct gravimetric determination of  $S$ . <sup>b</sup>  $S$  evaluated as  $P/D$ .<sup>c</sup>  $D = P/S$ . <sup>d</sup>  $D$  estimated directly via time-lag.**Table 5. Comparison of Calculated and Experimental Transport Properties<sup>a</sup>**

(a) PTMSS

solubility coefficient, $S$ [cm <sup>3</sup> (STP)/(cm <sup>3</sup> atm)]				selectivity:solubility ratio O <sub>2</sub> /N <sub>2</sub>	model (ref)
O <sub>2</sub>	N <sub>2</sub>	CO <sub>2</sub>	CH <sub>4</sub>		
0.31	0.18	2.17	0.58	1.72	PTMSS-1
0.3	0.17	2.01	0.56	1.77	PTMSS-2
0.36	0.21	2.8	0.7	1.71	PTMSS-3
0.275	0.175	2.6	0.68	1.57	(18)

diffusion coefficient, $D$ [10 <sup>-7</sup> cm <sup>2</sup> /s]				selectivity:diffusion ratio O <sub>2</sub> /N <sub>2</sub>	model (ref)
O <sub>2</sub>	N <sub>2</sub>	CO <sub>2</sub>	CH <sub>4</sub>		
82	44	12.5	27	1.86	PTMSS-1
83	39	13.6	24	2.13	PTMSS-2
66	40	8.4	23	1.65	PTMSS-3
15.5	7	6.6	3.9	2.21	(18)

(b) PFPDMSS

solubility coefficient, $S$ [cm <sup>3</sup> (STP)/(cm <sup>3</sup> atm)]				selectivity:solubility ratio O <sub>2</sub> /N <sub>2</sub>	model (ref)
O <sub>2</sub>	N <sub>2</sub>	CO <sub>2</sub>	CH <sub>4</sub>		
0.42	0.26	3	0.8	1.62	PFPDMSS-1
0.35	0.2	2.7	0.69	1.75	PFPDMSS-2
0.35	0.2	2.5	0.66	1.75	PFPDMSS-3
0.147	0.089	1.9	0.32	1.65	(18)

diffusion coefficient, $D$ [10 <sup>-7</sup> cm <sup>2</sup> /s]				selectivity:diffusion ratio O <sub>2</sub> /N <sub>2</sub>	model (ref)
O <sub>2</sub>	N <sub>2</sub>	CO <sub>2</sub>	CH <sub>4</sub>		
53	22	5.3	13.2	2.41	PFPDMSS-1
70	32	7.2	17.7	2.19	PFPDMSS-2
84	40	8.7	19.7	2.10	PFPDMSS-3
20	10	11.4	5.2	2.00	(18)

<sup>a</sup>  $P$  and  $D$  measured with a time-lag apparatus;  $S$  measured gravimetrically.

cal complication has to be considered. For "normal" models of about 3000–5000 atoms the Gusev–Suter module of the InsightII/Discover Software (cf. ref 29) usually permits a rather fine step width of 0.3 Å for the particle insertion grid superimposed onto the respective packing model. For the larger models used here only step widths of 0.5–0.75 Å were possible for numerical

reasons, which may lead to additional systematic errors particularly for the simulated  $D_{\text{calcd}}$  values.

The evaluation of Table 4 proves that all simulated PTMSP data are well in line with the experimental values. There is, however a significant difference between PTMSP-1, on one hand, which shows lower diffusivities than measured ones and PTMSP-2 and PTMSP-3, on the other hand, with relatively high  $D_{\text{calcd}}$  values.

It is obvious from Table 4 that simulated diffusion coefficients  $D_{\text{calcd}}$  in PTMSP vary rather significantly: e.g., for O<sub>2</sub> depending on a model, it is in the range (3.6–10.6) 10<sup>-5</sup> cm<sup>2</sup>/s. For all four gases and in three models, the mean deviation of  $D_{\text{calcd}}$  from the average  $D$  values is about 30%. Note that smaller deviations are observed for the two styrene polymers (Table 5, parts a and b). Presumably, the latter finding can be related to larger scale of nonuniform packing in the case of PTMSP, which means that the PTMSP models are still relatively small considering the size of individual free volume elements (see below).

These results can be compared with the experimental  $D$  values of PTMSP (Table 4). Several features of this material (tendency to fast aging, film thickness effects and so on) induce usually a wide range of experimental diffusivity (and permeability) values reported by different researchers. It can be seen from Table 4 that the  $D_{\text{exptl}}$  values of different gases also vary significantly depending on the PTMSP samples and the method used for evaluation of diffusivity. Of course, the reasons for variation of simulated and experimental  $D$  values are different. Nevertheless, the ranges of reported  $D_{\text{exptl}}$  and simulated in this work  $D_{\text{calcd}}$  values overlap quite well.

It should also be noted that the simulated solubility coefficients are much more consistent with the experimental ones; the variation of the models hardly influences the calculated  $S$  values.

Experimental gas permeability coefficients  $P$  are usually determined with better accuracy than diffusion coefficients. In addition, the  $P$  values are much more abundant in the literature, so better comparison of simulated and experimental values is possible. The three PTMSP models predict permeability coefficients of oxygen in the range of 6400–19400 barrer. Permeability coefficients of CO<sub>2</sub> that can be computed for the three models are 10000–50000 barrer. Both ranges are consistent with the experimental values reported by various researchers.<sup>41</sup> In judging these values it has to be considered that simulated permeabilities are obtained from the calculated  $S$  and  $D$  values using the well-known  $P = DS$  equation which leads to accumulation of errors.

At the end of the discussion of the  $S$  and  $D$  predictions for PTMSP, it is to be noticed that the good coincidence found between the calculated Gusev–Suter diffusivity data and experimental values at first glance is quite surprising. The Gusev–Suter method assumes that the diffusing particles follow a random walk through the polymer matrix. One might now think that in the continuous hole phase present in PTMSP the diffusion might not occur via individual jump events at all. A closer inspection of the distribution of the in most cases more than 300 sites of low probe molecule insertion energy (per volume of a packing cell) over the free volume of a PTMSP packing model does however show that most of these sites are located within the continuous part of the free volume (similar to zeolites mostly

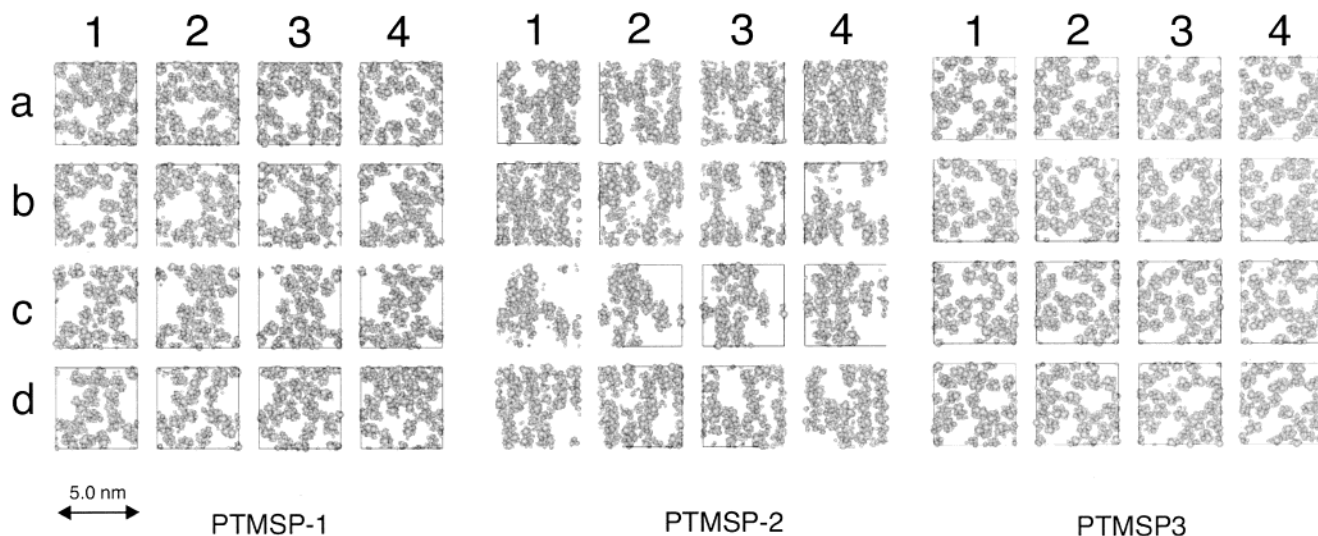


**Figure 1.** Representation of the free volume of the completely equilibrated PTMSP packing models as series of 3.11 Å thick slices cut perpendicular to the  $z$ -axis. 1a is the first and d4 is the last slice in each case.

near the lateral walls). The particle diffusion does then widely occur via jumps between these sites of local minimum insertion energy, which together with the also laterally large extension of the continuous hole phase accounts for the obvious applicability of the Gusev–Suter method for PTMSP.

In the cases of PTMSS (Table 5a) and PFPDMSS (Table 5b), all simulated solubilities are reasonably close to the respective experimental data. This indicates that the amount and distribution of the free volume which are of interest here are representative for the “real” materials. The  $S_{\text{calcd}}$  values are even closer to experiment for PTMSS than for PFPDMSS. This may be connected with experimental problems or with the fact that only PFPDMSS contains fluoride. As already mentioned even relatively small errors in the force field parametrization of fluorine atoms could also lead to some of the observed differences.

For all PFPDMSS models, all simulated diffusivities are also sufficiently consistent with the experiment. Only for PTMSS are the majority of  $D_{\text{calcd}}$  values by a factor of up to 7 higher than the measured results. Considering the reasonable behavior of the solubilities for the PTMSS models and the remark made above concerning the rather large step width which had to be used for the Gusev–Suter method, this finding should constitute no problem for detailed investigations of the free volume.

Deviations of simulated coefficients from average values for the three models in both styrene polymers are rather small: about 6% for PTMSS and 11% for PFPDMSS.

When considering all three polymers examined, it can be concluded that simulated and measured solubility coefficients change for the gases ( $\text{N}_2$ ,  $\text{O}_2$ ,  $\text{CH}_4$ ,  $\text{CO}_2$ ) in a “correct” manner; that is, they correlate with condensability of penetrants as expressed by boiling points  $T_b$  or critical points  $T_c$ . Due to the already mentioned reduced accuracy of the simulated diffusivities, it does not make sense to consider respective trends in gas diffusivity.

**4.2. Visualization of Free Volume.** Figure 1 shows the free volume distribution at the experimentally obtained density of 0.75 g/cm<sup>3</sup> for the three PTMSP packing models as series of 3.11 Å thick slices cut

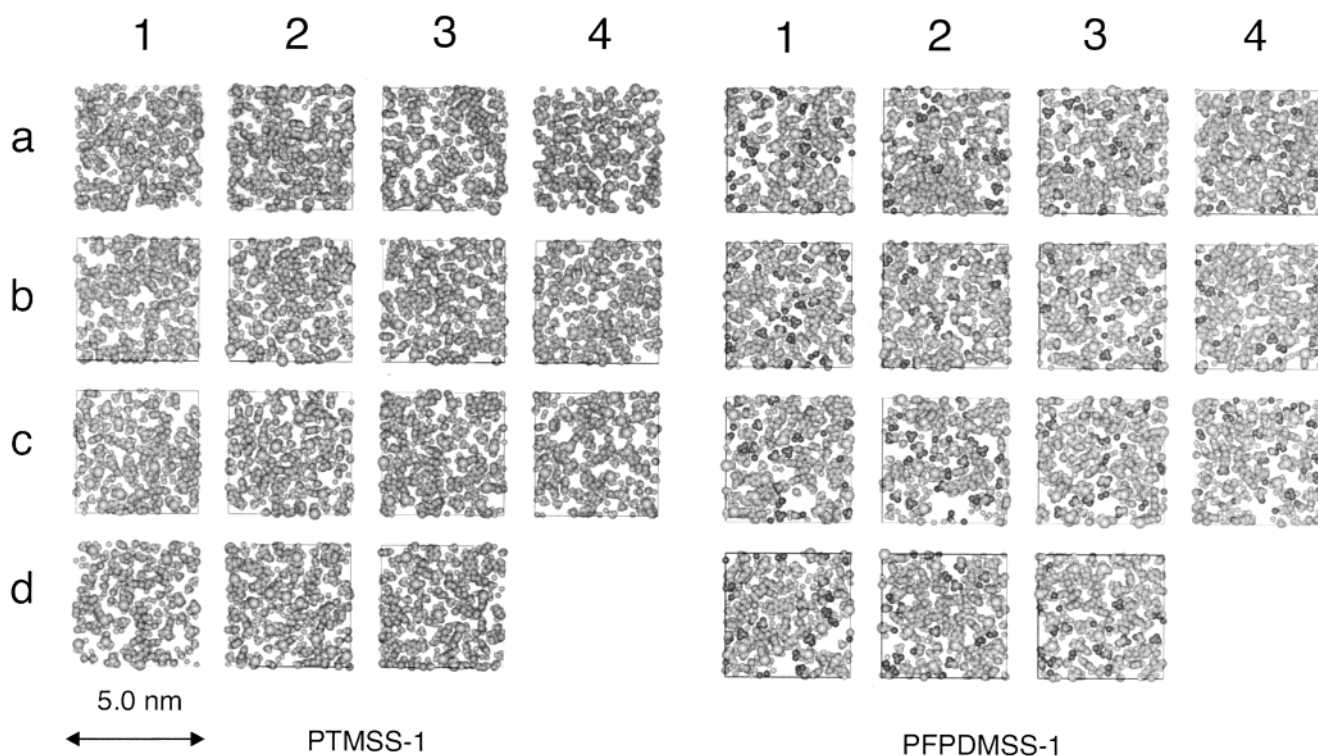
perpendicular to the respective  $z$ -axis. Considering the views shown there, it is necessary to recognize that PTMSP chains, due to their high intrinsic stiffness, look like sticks over very long distances (more than 10 nm). Thus the slice representations shown for PTMSP-1 and PTMSP-3 just happened to be oriented roughly perpendicular to the cut chain segments while in the case of PTMSP-2 the cut was roughly in parallel to the locally arranged chains.

Figure 2 shows similar representations for the models PTMSS-1 (slice thickness 3.0 Å) and PFPDMSS-1 (slice thickness 3.05 Å) being representative also for the other packing models of the respective polymers.

One can observe important qualitative differences in the amount and distribution of free volume in PTMSP, on one hand, and PTMSS and PFPDMSS, on the other hand. While the latter two materials show a widely homogeneous distribution of free volume which is quite typical for “normal” amorphous polymers with small and medium amounts of free volume,<sup>21,24,33</sup> PTMSP behaves differently.

This material obviously, on one hand, contains regions of high segmental packing density where the free volume distribution resembles the one in low and medium free volume polymers. On the other hand, rather large voids are present with a tendency to a partly continuous hole phase with lateral void widths between about 5 and 20 Å. This is in line with experimental data mentioned above. In the utilized models of limited size, this tendency to a continuous free volume phase is reflected by the presence of lengthy holes extending from one side of a model to the other, which considering the periodic boundary conditions leads to effectively infinite hole sizes.

A more attentive examination of the slices of the PTMSP cubes shown in Figure 1 reveals that some of larger holes have shapes that differ dramatically from spherical symmetry. For example, a hole shown in the slice a1 (PTMSP-1) with a cross-section of about 18 Å goes along the  $z$ -axis of the cube to the depth at least 50 Å (down to the slice d4). It means that larger microcavities have distinctly elongated shape. One can observe branchings of these “pores” in several cases. A comparison of several slices shows that local density can



**Figure 2.** Representation of the free volume of the completely equilibrated PTMSS-1 and PFPDMSS-1 packing models as a series of 3.0 and 3.05 Å, respectively, thick slices cut perpendicular to the  $z$ -axis. 1a is the first and d4 is the last slice in each case.

be quite large in some slices (cf. slice a1 for PTMSP-1 or slices a4 and b1 for PTMSP-2).

As was mentioned before, the structures of PTMSS and PFPDMSS look entirely different. Aside from the much smaller total free volume, it can be noted that the microcavities have shapes much closer to spherical symmetry. In most cases, a microcavity shown in one slice disappears on the next one; that is, the average size of a free volume element is often comparable with the distance between slides, i.e., about 3 Å.

It is of interest to compare these findings with the results of the studies of free volume in polymers using positron annihilation techniques. The very first study of free volume in PTMSP using PALS method<sup>13</sup> showed that much longer lifetimes and much larger sizes of free volume elements (radii  $R_4$  about 6 Å), if compared with conventional polymers, are characteristic for this polymer. In addition, "normal" radii of about 3.5 Å were also observed. Subsequent studies showed<sup>14,42,43</sup> that if measurements are performed in the absence of sorbed oxygen, when an additional channel for  $o$ -positronium decay can take place, the observed lifetimes and radii are even larger: the latter are equal to about 7 Å. Therefore, the size distribution of free volume in this polymer has a more complicated structure than the Gaussian form usually observed for conventional glassy polymers. Note that the size distribution in conventional glassy polymers becomes broader too, if the average size of free volume elements increases due to variation of the structure of chemically related polymers,<sup>44</sup> changes in temperature,<sup>45</sup> or the effects of pressure.<sup>46</sup> It can be reminded here that for the evaluation of positron annihilation experiments usually just spherical voids are considered with larger lengthy holes being replaced by a number of spheres of different size. So often no

perfect quantitative coincidence between results of molecular simulation and PALS data can be expected.

Concerning the above-mentioned presence of regions of rather high segmental packing density a theory reported by Doghieri et al.<sup>47</sup> is to be mentioned. It is based on a "nonequilibrium lattice fluid" (NELF) model for the description of thermodynamic properties of small molecules dissolved in glassy polymers. This theory for PTMSP also indicates the presence of densely packed domains with a density of about 1.25 g/cm<sup>3</sup>. This last mentioned value was obtained from a fit of the model to measured sorption isotherms. The presence of densely and loosely packed domains is also consistent with the assumptions of semiempirical dual mode sorption model, which gives an excellent fit of all the sorption data in glassy polymers.<sup>48</sup>

To arrive at a more quantitative description of the free volume distributions in the simulated model the following procedure was developed.

**4.3. Fractional Free Volume Determination.** For a further characterization of the fractional free volume, the nine equilibrated packings of the three polymers have been investigated in the following way. The atoms of the polymer chain have been assumed to be represented by hard spheres with a radius derived from the van der Waals radius of respective atoms (C, 1.55 Å; H, 1.10 Å; N, 1.40 Å; O, 1.35 Å; F, 1.30 Å; Si, 2.20 Å). To determine the FFV, the cubic packings were overlaid by a three-dimensional grid with a starting grid size  $\Delta$  of about 0.7 Å. At every grid point it was then tested if a hard sphere with the volume  $V_{\text{test}} = \delta^3$  (i.e.,  $r_{\text{test}} = 0.62035\delta$ , which is the smallest reasonable probe molecule radius considering the chosen grid width  $\delta$ ) would overlap with the hard spheres at the atom positions of the polymer. In the given case, the test particle for the

**Table 6. Fractional Free Volume (FFV) for PTMSP, PTMSS, and PFPDMSS Determined from Simulation<sup>a</sup>**

polymer	probe molecule radius $r_{\text{test}}/\text{\AA}$	fractional free volume
PTMSP	1.1	0.211 <sup>b</sup>
	0.43	0.369
	0.18	0.469
	extrapolated to zero	≈0.50
PTMSS	1.1	0.020 <sup>b</sup>
	0.43	0.185
	0.18	0.331
	extrapolated to zero	≈0.36
PFPDMSS	1.1	0.018 <sup>b</sup>
	0.43	0.188
	0.18	0.338
	extrapolated to zero	≈0.37

<sup>a</sup> The deviations of the FFV values for the individual packing models from the respective average value were between 0 and 3.5%. <sup>b</sup> Respective results obtained using the standard triangulation method of the Cerius2 software<sup>55</sup> are as follows: 0.25 for PTMSP, 0.026 for PTMSS, and 0.020 for PFPDMSS.

**Table 7. Fractional Free Volume Calculated Using the Bondi Method with Different Increments in the van der Waals Volume**

polymer	FFV	
	Askadskii <sup>50</sup>	Van Krevelen <sup>49</sup>
PTMSP	0.327	0.290
PTMSS	0.197	0.171
PFPDMSS	0.180	0.180

FFV had a radius of about 0.43 Å. The FFV accessible for these probe molecules was then estimated by the ratio of grid points without overlap to the total number of grid points. The procedure was repeated for a lattice spacing  $\delta$  of 0.3 Å and probe molecule radius of 0.18 Å<sup>2</sup>. Also a case with a lattice spacing  $\delta$  of 0.7 Å and probe molecule radius of 1.1 Å<sup>2</sup> (the size of a positronium molecule) was considered. The FFV obtained in this way does of course depend on the utilized probe molecule radius. Table 6 contains the respective results together with the FFV obtained from an extrapolated probe molecule radius of zero. It should be noticed that the zero radius FFV values consider even the most minute spaces not filled by polymer atoms.

The results of the simulated FFV shall now be compared with the rough estimations of this value using the Bondi method. It is known that the arbitrariness of this approach can be caused by the assumption of a universal relation between van der Waals volume  $V_w$  and occupied volume  $V_{oc}$ :

$$V_{oc} = 1.3 V_w \quad (2)$$

Another reason for variations of the FFV values found in this manner and typically observed poor correlation with observed parameters such as diffusion coefficients can be related to different scales for the increments in  $V_w$ . The FFV values found using the increments given by Van Krevelen<sup>49</sup> and Askadskii<sup>50</sup> are compared in Table 7.

The best coincidence between the simulated, presumably more accurate, FFV values and the Bondi data is obtained for the medium size probe molecule radius of 0.43 Å, while the FFV values extrapolated to a probe radius size of zero are considerably higher. That obviously means that when the "universal" scaling factor for  $V_w$  of 1.3 is used in the Bondi method the most minute spaces not filled by polymer atoms seems to be escaped from the consideration.

The FFV values obtained from a zero probe molecule radius for PTMSS and PFPDMSS given in Table 6 may look a bit high in comparison with the visual views on these polymers provided in Figure 2. However, one has to consider the fact that even in the closest possible hexagonal packing of spheres of equal radius the unoccupied volume is 26%. That means that although a hexagonal packing of spheres is not exactly the same as a packing of polymer chain segments, many very minute "hard to see" unoccupied volume elements can mount up to a considerable overall effect.

It will be interesting also to determine the FFV by molecular modeling for other polyacetylenes some of which showed unusual density and FFV values estimated via the Bondi method.<sup>51</sup>

**4.4. Size Distribution of Free Volume Elements (FVE).** While the FFV characterized only the overall amount of the free volume, the size distribution of the free volume regions should be more characteristic for specific polymers. It is clear that the resulting distribution will depend on the size of the test particle which scans the free volume regions. The applied methods to obtain free volume data from the experimentally observed PALS spectra due to respective corrections are supposed to be related with the real size of holes starting from a cutoff radius of about 1.1 Å which is the size of a positronium molecule.

The free volume of the simulated packing models of the investigated polymers was determined by superimposing a grid of a grid step width  $\delta = 0.7$  Å with a probe molecule radius of 1.1 Å (size of positronium atom). As in the case of the FFV determination discussed above, at every point of the  $\delta$  grid a test was made to see if an overlap occurs between the test particle and any hard sphere atom of the polymer when the center of the hard sphere test particle is sitting on the grid point. The result is a classification of grid points as "occupied" or "free". Next, the connectivity of the "free" grid points was considered and connected "free" grid points were collected into groups, which were labeled with a specific number. This was done in two ways. In the first approach (named V\_connect), it was tested if a still unlabeled "free" grid point has a "free" grid point as next neighbor. If yes, and if this neighbor belongs already to a labeled group, the considered point belongs to the same group as the neighbor point. Otherwise, the two points are the origin of a new group of points. Considering all "free" grid points in this way allows a partitioning of "free" grid points into separate sets. The number of points in each set times the volume of a  $\delta^3$  cubicle was used as a measure for the volume of a region accessible by the center of the test particle. Thus, this approach identifies the holes by a simple topological criterion.

In the second approach (named R\_max), the precalculated information of the "shortest distance" from every grid point to its closest polymer atom was used to group every "free" grid point. The points were assigned to the closest point with a local maximum value of this "shortest distance". These local maximum points were found by an iterative loop. Starting from a selected "free" grid point, the gradient of the change of the "shortest distance" belonging to every "free" neighbor point was calculated. The R\_max approach may dissolve larger FVE regions of elongated or highly complex shape into smaller "local" regions, as is shown schematically in Figure 3.

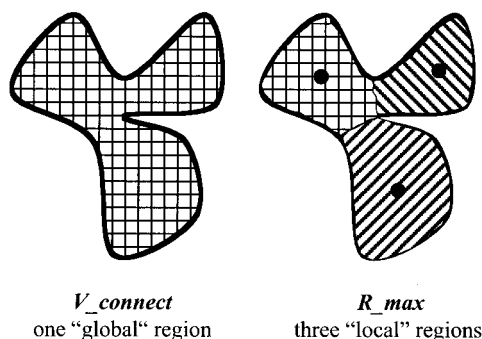


**Figure 3.** Principal view of the two approaches to connect free grid points in an example free volume region. In  $V_{\text{connect}}$  (left), all connected "free" grid points belong to one region. In the  $R_{\text{max}}$  approach (right), first points of local maxima of "shortest distances" to polymer atoms are determined (dots), and then the grid points are assigned. The result is a decomposition into three more local regions.

It is assumed that this approach to the determination of free volume distributions is more suited for comparisons with PALS data. For instance, it can be seen from reported PALS data for PTMSP in the literature<sup>13,14,42,43</sup> that the experimentally determined hole sizes clearly show an upper limit somewhere above a hole radius of 8 Å. That means, the positronium probe molecules do not "see" extended holes or holes of complex shape as single entities. These holes are obviously broken down to smaller holes of less complex shape. Therefore, in the following, the  $R_{\text{max}}$  method will be used for all comparisons with PALS data.

As in the case of  $V_{\text{connect}}$ , in the  $R_{\text{max}}$  approach, the volume of each region of connected grid points was also approximated by the number of the points times the volume of a  $\delta^3$  cubicle. Due to the fact that the analysis of the experimental PAL data assumes a spherical shape of the free volume elements, all FVE size distributions shown in the following figures are represented as a function of the radius of spheres with the same volume as the respective "real" free volume regions. Since the sphere radius of a given hole as it would be obtained from the grid points where a positronium molecule can reside without any overlap with the boundaries of the hole, the real size of the hole would be underestimated in comparison to PALS. Therefore a correction was applied to the calculated hole radii by adding the radius of positronium atom of 1.1 Å to each sphere radius.

The resulting distribution functions for PFPDMSS, PTMSS, and PTMSP calculated with the  $R_{\text{max}}$  approach and statistically weighted with the volume of the respective hole, are presented in Figures 4–6. For comparison, Figure 7 contains the respective FVE size distribution based on the  $V_{\text{connect}}$  method for PTMSP.

For each polymer the distribution was determined from the three packing models (see Tables 4 and 5) used in the calculation of transport properties. In particular, for PTMSP, the resulting distributions at the given sampling of 1.1 Å for the respective probe molecule size still show strong fluctuations and also voids. This is due to the fact that although the utilized models for PTMSP are much larger (about 50 Å side length) than in other studies of this material previously reported in the literature,<sup>22,23</sup> the model size is still not optimal for this ultrahigh free volume material. Therefore, a simple five-point smoothing was applied. The resulting smoothed distributions are also shown in Figures 4–7.

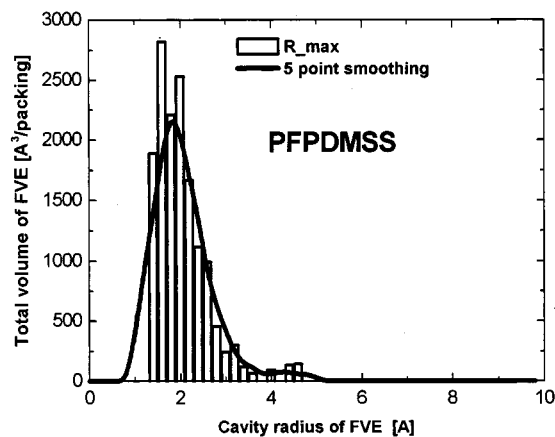


**Figure 4.** Size distribution of free volume elements (FVE) for PFPDMSS as a function of cavity radius of spheres of equivalent volume averaged over the three packing models. The  $R_{\text{max}}$  method was applied.

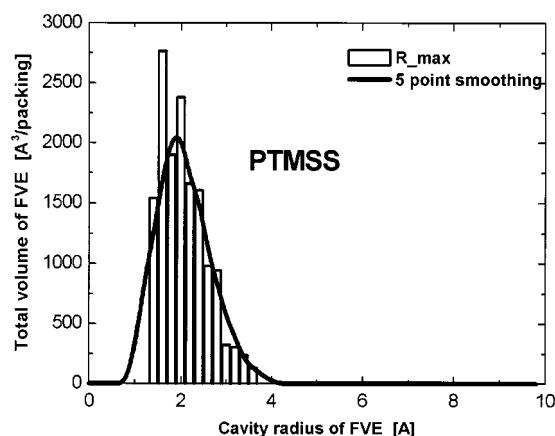


**Figure 5.** Size distribution of free volume elements (FVE) for PFPDMSS as a function of cavity radius of spheres of equivalent volume averaged over the three packing models. The  $R_{\text{max}}$  method was applied.

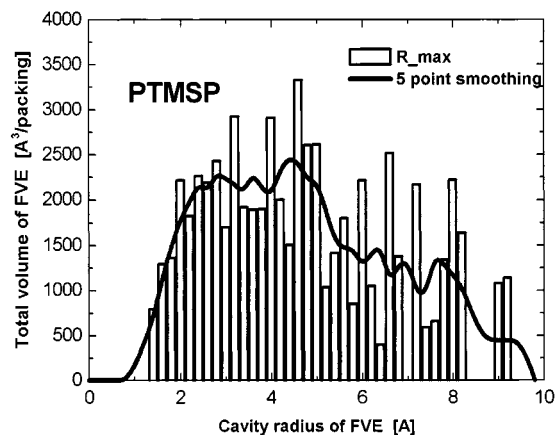


**Figure 6.** Size distribution of free volume elements (FVE) for PFPDMSS as a function of cavity radius of spheres of equivalent volume averaged over the three packing models. The  $R_{\text{max}}$  method was applied.

The following free volume properties are obtained from the modeling results. PTMSP has a much wider range of cavity sizes (radius: 1.1 to about 9 Å) than PFPDMSS (radius: 1.1–4.5 Å), and PTMSS (radius: 1.1–4.0 Å). Furthermore, the computer simulation predicts for PTMSP (cf. Figure 6) an asymmetric distribution with at least two peaks, one at about 3–4

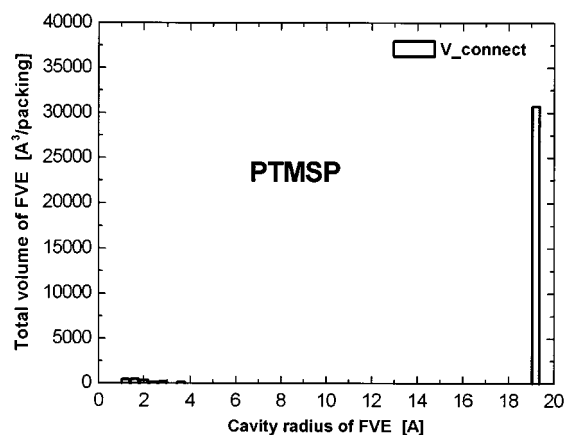


**Figure 7.** Size distribution of free volume elements (FVE) for PFPDMSS as a function of cavity radius of spheres of equivalent volume averaged over the three packing models. The  $V_{\text{connect}}$  method was applied.

Å and one (appearing as a shoulder) between about 6 and 8 Å. This result reflects again the intuitive image one gets from observing slice pictures of a PTMSP packing models (cf. Figure 1) which showed a larger number of small voids in this polymer and in addition regions composed of very large free volume elements.

The smoothed distribution for PFPDMSS (cf. Figure 4) shows one major peak with a peak maximum at about 2 Å. Also, PTMSS shows only a single peak with a maximum at about 2 Å.

Figure 7, which contains the distribution of complete holes ( $V_{\text{connect}}$ ), underlines the fact that in PTMSP most of the free volume is organized in a continuous hole phase. This is indicated by the dominating very large peak at 19 Å. Here it has to be mentioned that due to the calculation scheme utilized (cf. above) this average diameter value only refers to the free volume organized in the continuous free volume phase in the respective basic volume elements of a lateral dimension of about 5 nm. The position of this peak would, thus, increase with increasing model size, reaching infinity for a model of infinite size. In this regard, it is interesting to compare this finding with the maximum distance of a constituent lattice point of this extended free volume region, which for the three simulated PTMSP models is on average at  $8.3 \pm 0.9$  Å. This clearly underlines the highly nonspherical shape of this free volume phase. It also provides an additional argument for using a description of the free volume distribution which splits larger lengthy holes of complex geometry into smaller more compact ones.

Now the results of computer simulation shall be compared in more detail with the findings of the study of these polymers using positron annihilation lifetime spectroscopy. Figure 8 presents lifetime distribution observed for PTMSP and PFPDMSS. The distribution of PTMSS is virtually identical with that of PFPDMSS, and so it is not shown. The positronium peak of PFPDMSS corresponding to the longest lifetime is broader than the typical peak CONTIN program produces in studies of conventional glassy polymers such as, e.g., poly(methyl methacrylate).<sup>52</sup> It should be noted that it does not allow one to split this peak into two components with different lifetimes as finite-term PATFIT program describes free volume of this polymer.<sup>18</sup> On the other hand, CONTIN lifetime distribution of

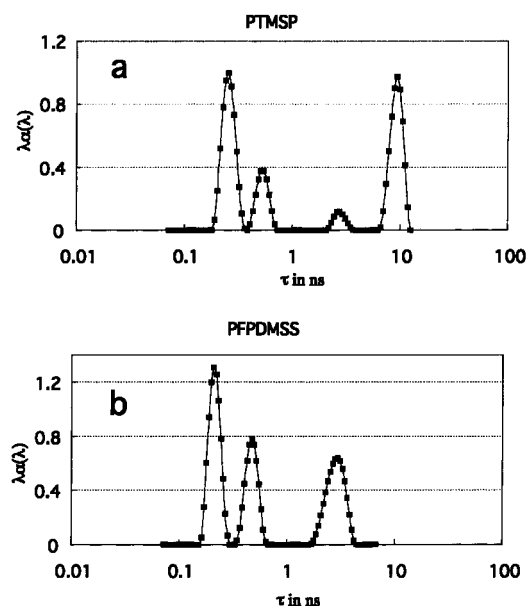


**Figure 8.** PALS lifetime distribution observed for PTMSP and PFPDMSS.

PTMSP reveals two distinctive peaks with the maxima of 2.7 and 10.9 ns.

Using the Tao–Eldrup equation (see ref 53), the lifetime distributions were converted in the free volume size distributions of these two polymers. They are shown in Figure 9. As already found by computer modeling, the FVE size distribution of PTMSP based on PALS measurement is much wider as compared to that of PFPDMSS and other conventional glassy polymers. It indicates the existence of microcavities as small as 2 Å and as large as 8 Å in the structure of this polymer. Both approaches show that bimodal size distribution gives much a better description than monomodal (usually Gauss type) distribution observed for glassy polymers (see, e.g., refs 44 and 45). For PTMSP the major difference between simulated and measured free volume distributions consists of the fact that the ratio between the areas of the peaks for the smaller and the larger holes is much larger in the case of the simulated data (cf. Figure 6) than in the case of the measured data (cf. Figure 9). This most likely indicates differences in the statistical weights applied to both types of distributions. This problem will need further studies.

For PFPDMSS the single peak of size distribution is located at significantly smaller radii. However, for this polymer the maximum of FVE size distribution deduced from computer modeling (2 Å) is smaller than the one found in the PALS experiments (3.6 Å). Also this discrepancy should be a subject of further studies. A possible reason could consist of a different behavior of positronium probe molecules in the small holes of these specific modified polystyrenes than in PTMSP. This could lead to problems with the application of the correction term  $\Delta R$  utilized in the Tao–Eldrup model<sup>53</sup> (cf. also Goworek<sup>54</sup>).

Finally it should be mentioned that the model PTMSP-1 which showed considerably smaller (although still acceptable) diffusion coefficients than PTMSP-2 and PTMSP-3 (cf. Table 4) did not reveal severe differences in its free volume characteristics in comparison to the other two PTMSP models. It implies, therefore, that the differences in the simulated diffusion coefficients are

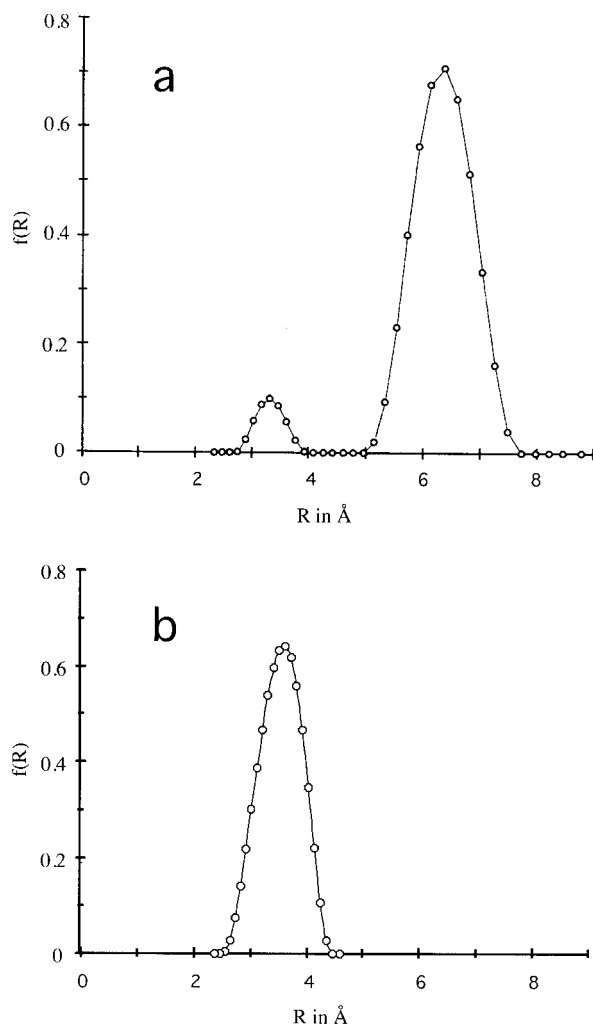


**Figure 9.** Free volume element (FVE) size distributions for PTMSP and PFPDMSS obtained from lifetime distributions using the Tao–Eldrup equation.

caused mainly by variations in the packing of chain segments between the holes.

## 5. Summary

Results of positron annihilation lifetime spectroscopy (PALS) and molecular modeling on the free volume distribution in an ultrahigh free volume material (PTMSP) and two more conventional amorphous polymers (modified polystyrenes PFPDMSS and PTMSS) were compared.

Important differences in the distribution of free volume in high and low free volume polymers could be characterized in detail.

The main focus of the work was on the molecular modeling approach. Extended equilibration procedures were necessary to obtain reasonable packing models for the polymers. The transition state Gusev–Suter Monte Carlo method was utilized to prove a reasonable agreement between simulated and measured diffusivity and solubility values for the model structures. The free volume distribution of the created model structures was analyzed using an approach that splits larger lengthy holes of complex geometry in smaller ones of more compact shape. The resulting free volume distribution from the simulation as well as the experimental PALS investigation resulted in an at least bimodal distribution of free volume for PTMSP while the polystyrene deriva-

tives as other conventional glassy polymers showed a more or less monomodal behavior.

**Acknowledgment.** We would like to acknowledge that parts of the work were supported by the European Commission “Growth” Program, “PERMOD—Molecular modeling for the competitive molecular design of polymer materials with controlled permeability properties”, Contract #G5RD-CT-2000-200, and by the INTAS–RFBR 97–1525 grant.

## References and Notes

- (1) Victor, J. G.; Torkelson, J. M. *Macromolecules* **1987**, *20*, 2241–2250.
- (2) Wasserman, A. M.; Kovarskii, A. L. *Spin Probes And Labels in Physical Chemistry of Polymers*; Nauka: Moscow, 1986.
- (3) Yampolskii, Yu. P.; Kaliuzhnyi N. E.; Durgaryan, S. G. *Macromolecules* **1986**, *19*, 846–851.
- (4) Shrader, D. M.; Jean Y. C., Eds.; *Positron and Positronium Chemistry*; Elsevier: Amsterdam, 1988.
- (5) Masuda, T.; Isobe, E.; Higashimura, T. *J. Am. Chem. Soc.* **1983**, *105*, 7473–7474.
- (6) Masuda, T.; Isobe, E.; Higashimura, T. *Macromolecules* **1985**, *18*, 841–845.
- (7) Stern, S. A. *J. Membr. Sci.* **1994**, *94*, 1–65.
- (8) Masuda, T.; Iguchi, Yu.; Tang, B.-Z.; Higashimura, T. *Polymer* **1988**, *29*, 2041–2049.
- (9) Morisato, A.; Shen, H.-C.; Sankar, S.; Freeman, B. D.; Casillas, C. G.; Pinau, I. *J. Polym. Sci., Part B: Polym. Phys.* **1996**, *34*, 2209–2222.
- (10) Ichiraku, Y.; Stern, S. A.; Nakagawa, T. *J. Membr. Sci.* **1987**, *34*, 5–18.
- (11) Plate, N. A.; Bokarev, A. K.; Kaliuzhnyi, E. G.; Litvinova, V. S.; Khotimskii, V. S.; Volkov, V. V.; Yampol'skii, Yu. P. *J. Membr. Sci.* **1991**, *60*, 13–24.
- (12) Langsam, M.; Robeson, L. M. *Polym. Eng. Sci.* **1989**, *29*, 44–54.
- (13) Yampolskii, Yu. P.; Shantarovich, V. P.; Chernyakovskii, F. P.; Kornilov, A. I.; Plate, N. A. *J. Appl. Polym. Sci.* **1993**, *47*, 85–92.
- (14) Consolati, G.; Genko, M.; Pegoraro, M.; Zanderighi, L. *J. Polym. Sci., Polym. Phys.* **1996**, *34*, 357–367.
- (15) Savoca, A. C.; Surnamer, A. D.; Tien, C. *Macromolecules* **1993**, *26*, 6211–6216.
- (16) Costa, G.; Grosso, A.; Sacchi, M. C.; Stein, P. C.; Zetta L. *Macromolecules* **1991**, *24*, 2858–2861.
- (17) Clough, S. B.; Sun, X. F.; Tripathy S. K.; Baker, G. L. *Macromolecules* **1991**, *24*, 4264–4269.
- (18) Khotimskii, V. S.; Filippova, V. G.; Bryantseva, I. S.; Bondar, V. I.; Shantarovich, V. P.; Yampolskii, Y. P. *J. Appl. Polym. Sci.* **2000**, *78*, 1612–1620.
- (19) Müller-Plathe, F. *Acta Polym.* **1994**, *45*, 259–293.
- (20) Gusev, A. A.; Müller-Plathe, F.; van Gunsteren, W. F.; Suter, U. W. *Adv. Polym. Sci.* **1994**, *16*, 207–247.
- (21) Hofmann, D.; Fritz, L.; Ulbrich, J.; Schepers, C.; Böhning, M. *Macromol. Theory Simul.* **2000**, *9*, 293–327.
- (22) Fried, J. R.; Goyal, D. K. *J. Polym. Sci., B: Polym. Phys.* **1998**, *36*, 519–536.
- (23) Madkour, T. M. *Polymer* **2000**, *41*, 7489–7497.
- (24) Nagel, C.; Schmidtke, E.; Günther-Schade, K.; Hofmann, D.; Fritsch, D.; Strunskus, T.; Faupel, F. *Macromolecules* **2000**, *33*, 2242–2248.
- (25) Hofmann, D.; Fritz, L.; Ulbrich, J.; Paul, D. *Polymer* **1997**, *38*, 6145–6155.
- (26) Hofmann, D.; Fritz, L.; Ulbrich, J.; Paul, D. *Comput. Theory Polym. Sci.* **2000**, *10*, 419–436.
- (27) Yampolskii, Yu. P.; Motyakin, M. V.; Wasserman, A. M.; Masuda, T.; Teraguchi, M.; Khotimskii V. S.; Freeman, B. D. *Polymer* **1999**, *40*, 1745–1752.
- (28) Schmitz, H.; Müller-Plathe, F. *J. Chem. Phys.* **2000**, *112*, 1040–1045.
- (29) *Polymer User Guide, Amorphous Cell Section, Version 4.0.0*; Molecular Simulations: San Diego, CA, 1996.
- (30) Sun, H.; Rigby, D. *Spectrochim. Acta* **1997**, *53A*, 1301–1323.
- (31) Rigby, D.; Sun, H.; Eichinger, B. E. *Polym. Int.* **1997**, *44*, 311–330.
- (32) Pullumbi, P. (Air Liquide (France)) Oral presentation at the Second International Workshop “Molecular Modelling in Membrane Research”, Teltow, Germany, March 17–19, 1999.

- (33) Tocci, E.; Hofmann, D.; Paul, D.; Russo, N.; Drioli, E. *Polymer* **2001**, *42*, 521–533.
- (34) Bondi, A. *Physical Properties of Molecular Crystals, Liquids, and Glasses*; Wiley: New York, 1968.
- (35) Park, J. Y.; Paul, D. R. *J. Membr. Sci.* **1997**, *125*, 23–39.
- (36) Gregory, R. B.; Yongkang, Zhu. In *Positron and Positron Chemistry*; Jean, Y. C., Ed.; World Scientific: Singapore, 1991; p 136.
- (37) Provensher, S. W. *Comput. Phys. Commun.* **1982**, *27*, 229.
- (38) Gusev, A. A.; Arizzi, S.; Suter, U. W. *J. Chem. Phys.* **1993**, *99*, 2221–2227.
- (39) Gusev, A. A.; Suter, U. W. *J. Chem. Phys.* **1993**, *99*, 2228–2234.
- (40) Bondar, V. I. Ph.D. Thesis, Institute of Petrochemical Synthesis, 1995.
- (41) Nagai, K.; Freeman, B. D.; Hill, A. J. *J. Polym. Sci., B: Polym. Phys.* **2000**, *38*, 1222–1239.
- (42) Shantarovich, V. P.; Kevdina, I. B.; Yampolskii, Yu. P.; Alentiev, A. Yu. *Macromolecules* **2000**, *33*, 7453–7466.
- (43) Consolati, G.; Rurali, R.; Stefanetti, M. *Chem. Phys.* **1998**, *237*, 493–499.
- (44) Jean, Y. C.; Yuan, J.-P.; Liu, J.; Deng, Q.; Yang, H. *J. Polym. Sci., Part B: Polym. Phys.* **1995**, *33*, 2365–2371.
- (45) Liu, J.; Deng, Q.; Jean, Y. C. *Macromolecules* **1993**, *26*, 7149–7155.
- (46) Deng, Q.; Jean, Y. C. *Macromolecules* **1993**, *26*, 30–34.
- (47) Doghieri, F.; Sarti, G. C. *Macromolecules* **1996**, *29*, 7885–7896.
- (48) Paterson, R.; Yampolskii, Yu.; Fogg, P. G. T. The Solubility of Gases in Glassy Polymers, IUPAC–NIST Solubility Data Series 70. *J. Phys. Chem. Ref. Data* **1999**, *28*, 1255.
- (49) Van Krevelen, D. W. *Properties of Polymers*, 3rd ed.; Elsevier: Amsterdam, 1990.
- (50) Askadskii, A. A. *Physical Properties of Polymers: Prediction and Control*; Gordon and Breach Publishers: Amsterdam, 1996.
- (51) Yampolskii, Yu. P.; Korikov, A. P.; Shantarovich, V. P.; Nagai, K.; Freeman, B. D.; Masuda, T.; Teraguchi, M.; Kwak, G. *Macromolecules* **2001**, *34*, 1788–1796.
- (52) Shantarovich, V. P.; Novikov, Yu. A.; Suptel, Z. K.; Oleinik, E. F.; Boyce, M. C. *Acta Phys. Polym., A* **1999**, *95*, 659.
- (53) Nakanishi, H.; Wang, S. J.; Jean, Y. C. In *Positron Annihilation Studies of Fluids*; Sharma, S. C., Ed.; World Science: Singapore, 1988; p 292.
- (54) Goworek, T. *J. Nucl. Radiochem. Sci.* **2000**, *1*, 11–13.
- (55) Geometry module of the Cerius2 software, version 4.6; Accelrys Ltd: San Diego, CA, 2001.

MA011360P